Theoretical & Applied Mechanics Letters 9 (2019) 84-95

Contents lists available at ScienceDirect

Theoretical & Applied Mechanics Letters

journal homepage: www.elsevier.com/locate/taml

Article

Numerical solutions for point masses sliding over analytical surfaces: Part 1

Glauco Gallotti*, Stefano Tinti

Department of Physics and Astronomy, University of Bologna, Bologna 40126, Italy

ARTICLE INFO

Article history:
Received 18 February 2019
Accepted 11 March 2018
Available online 11 March 2018
*This article belongs to the Solid Mechanics.

Keywords:
Point-mass sliding
Two point-mass systems
Analytical surfaces
Numerical methods
Runge–Kutta method

ABSTRACT

In this study, we introduce a system of differential equations describing the motion of a single point mass or of two interacting point masses on a surface, that is solved by a fourth-order explicit Runge–Kutta (RK4) scheme. The forces acting on the masses are gravity, the reaction force of the surface, friction, and, in case of two masses, their mutual interaction force. This latter is introduced by imposing that the geometrical distance between the coupled masses is constant. The solution is computed under the assumption that the point masses strictly slide on the surface, without leaping or rolling. To avoid complications stemming from numerical errors related to real topographies that are only known over discrete grids, we restrict our attention to simulations on analytical continuous surfaces. This study sets the basis for a generalization to more complex systems of masses, such as chains or matrices of blocks that are often used to model complex processes such as landslides and rockfalls. The results shown in this paper provide a background for a companion paper in which the system of equations is generalized, and different geometries are presented.

1 Introduction

The formal description of masses sliding on surfaces finds application in several science branches, from engineering to geophysics. Among the variety of possible applications, we focus our attention on large-scale phenomena, such as landslides, that are of primary importance, especially for hazard assessment analyses.

In general, landslides occur in a variety of forms. The simplest approach is to model a landslide as a rigid body or as a set of interacting blocks moving down a sloping surface. In most cases this is found to represent the landslide motion reasonably well for a broad range of phenomena [1-8]. Similarly, the block models are also used for predicting of the permanent displacements of natural slopes subject to seismic instability [9, 10]. Typically, the sliding body is portioned into a set of blocks sliding down a surface. The motion of each block is described by the motion of the projection of its center of mass moving on a surface. The dynamics of particles and of rigid bodies has been widely studied and investigated [11, 12]. In this paper, we follow the classical approach to describe the motion of a couple of masses over a two-dimensional (2D) surface. The forces acting on the particles are gravity, the reaction force of the surface, the basal friction and the interaction force. This latter is the core of this study and sets the basis for the extension to a more complex system composed of multiple masses and suitable for the description of landslides phenomena. We describe the particles' motion by means of a system of ordinary differential equations (ODE), solved through a series of assumptions we discuss in detail in Sect. 3.

To improve our understanding of the coupled-mass system, in Sect. 2 we propose simulations of the motion of a single mass sliding down a surface. In both cases, the assumption is made that the masses move remaining strictly adherent to the surface, i.e. that the masses can neither leap nor roll, but only slide down the surface.

As we have previously remarked, in the case of coupled masses, we introduce the interaction force. In this paper, we explore the dynamics of a system where this force is such that no elastic deformation is allowed through the joining line between the two particles. Formally, we can obtain this condition by imposing that the three-dimensional (3D) distance between the two masses is constant. This approach is commonly used in

* Corresponding author.
E-mail address: glauco.gallotti2@unibo.it (G. Gallotti).

http://dx.doi.org/10.1016/j.taml.2019.02.004

block models to avoid the overlapping between a block and its adjacent one [10]. Nevertheless, in this work, we use this geometrical bound to compute the system dynamics. Basically, the rigidity is not imposed as an added condition, but is a factor influencing the motion.

We consider only simulations on analytical surfaces of the type $z = f(x, y)$, where x and y are the horizontal coordinates and z is the vertical coordinate of a Cartesian reference frame. The motion equations imply first- and second-order derivatives of the surface f. Geometrically speaking, the line joining the masses is at any time a chord of the surface. In this paper we will solve the problem under the additional constraint that the angle between the chord and the plane tangent to the surface is small and we will show examples fulfilling such an assumption. The general case will be treated in detail in the companion paper. We believe that the two papers are needed in order to provide a better understanding of the process that leads to the general formulation. This latter can be ultimately applied to systems formed by a large number of interacting particles able to slide simultaneously. The innovation of this approach lies in the fact that the bounds among each couple of particles can be evaluated and studied anytime during the motion. Thus, in the forthcoming description of landslide processes, the sliding body can be modified ensuing hypotheses on the rock properties. These latter can be accounted in the terms of the interaction forces variations.

Sliding surfaces in real cases are known only on a discrete set of observation points, which implies that the related space derivatives can be computed only by means of discrete differential operators and can be obviously known only with less accuracy. Since our primary aim is to focus on the theoretical formulation of the problem and its adequacy to compute the motion of single as well as interacting masses, we consider only analytical surfaces here and leave the problem of the poor knowledge of the real topographical surfaces and of their derivatives to further studies. Pointedly, in this work we use an explicit fourth-order Runge–Kutta scheme (RK4) implemented through a MATLAB code. The RK methods have been widely studied and investigated [13], especially to solve systems of ordinary differential equations [14, 15].

In what follows we first formulate the problem for a single mass system (Sect. 2), then we extend the formulation to cover the case of two interacting mass constrained to lay at a constant distance from each other (Sect. 3).

2 Motion of a single mass

2.1 Formulation of the problem

In this section we formulate the problem of a single mass (a point mass) sliding on a generic analytical surface described by the equation $z = f(x, y)$, where the function $f(x, y)$ is of class C^2. We will first introduce the equations of motion in RK4. Eventually, we will show simulations for some selected surfaces.

Let us assume that the point mass slides under the effect of gravity $\boldsymbol{g}$ that in a Cartesian right-hand unit-vector system $\boldsymbol{i}, \boldsymbol{j}, \boldsymbol{k}$, with $\boldsymbol{k}$ directed upward, can be represented as

$$\boldsymbol{g} = -g\boldsymbol{k}. \tag{1}$$

Let us further introduce a local set of three orthonormal vectors $\boldsymbol{s}_1, \boldsymbol{s}_2, \boldsymbol{n}$, where $\boldsymbol{n}$ is normal to the surface and points upward, $\boldsymbol{s}_1$ is the maximum-steepness tangential vector (i.e. it belongs to the vertical plane determined by $\boldsymbol{n}$ and $\boldsymbol{k}$ and points upward), and $\boldsymbol{s}_2$ is the horizontal vector orthogonal to $\boldsymbol{s}_1$ and $\boldsymbol{n}$. In terms of the function f and its first derivatives f_x and f_y, the local unit-vector system can be given through the following expressions

$$\boldsymbol{s}_1 = \frac{1}{\left[f_x^2 + f_y^2 + \left(f_x^2 + f_y^2\right)^2\right]^{\frac{1}{2}}} \left(f_x,\, f_y,\, f_x^2 + f_y^2\right), \tag{2a}$$

$$\boldsymbol{s}_2 = \frac{1}{\left(f_x^2 + f_y^2\right)^{\frac{1}{2}}} \left(-f_y,\, f_x,\, 0\right), \tag{2b}$$

$$\boldsymbol{n} = \frac{1}{\left(1 + f_x^2 + f_y^2\right)^{\frac{1}{2}}} \left(-f_x,\, -f_y,\, 1\right). \tag{2c}$$

These three unit vectors form the basis of a right-hand Cartesian reference frame and degenerate only in the points of the surface where both derivatives f_x and f_y are equal to zero.

The gravity acceleration $\boldsymbol{g}$ can be represented in the local system and, noting that $\boldsymbol{g} \cdot \boldsymbol{s}_2 = 0$, takes the form

$$\boldsymbol{g} = g_s \boldsymbol{s}_1 + g_n \boldsymbol{n}, \tag{3}$$

where the components are given by $g_s = \boldsymbol{g} \cdot \boldsymbol{s}_1$ and $g_n = \boldsymbol{g} \cdot \boldsymbol{n}$.

The reaction force exerted by the surface on the moving point is directed along $\boldsymbol{n}$ and points upward/downward depending on the local concavity/convexity of the surface. Denoting the reaction acceleration by $R\boldsymbol{n}$, one can write the following equation for the acceleration of a point mass

$$\boldsymbol{a} = \boldsymbol{g} + R\boldsymbol{n} - \mu\,|R|\,\boldsymbol{v}. \tag{4}$$

Here, it is further assumed that the friction term is proportional to the surface reaction through the friction coefficient μ and is always directed against the instant unit velocity vector $\boldsymbol{v}$. If one designates the point acceleration component normal to the surface by a_n, i.e. $a_n = \boldsymbol{a} \cdot \boldsymbol{n}$, it is straightforward to deduce the expression for R. In fact, after dot multiplying both members of Eq. (4) by $\boldsymbol{n}$, and noting that $\boldsymbol{v} \cdot \boldsymbol{n} = 0$, one gets

$$R = a_n - g_n. \tag{5}$$

Considering the decomposition of Eq. (3) the governing equation for the point mass can be given the following form

$$\boldsymbol{a} = g_s \boldsymbol{s}_1 + a_n \boldsymbol{n} + \mu\,(g_n - a_n)\,\boldsymbol{v}. \tag{6}$$

It is known that the normal acceleration a_n can be expressed in terms of the point velocity and of the surface geometrical characteristics. For example, one can write $a_n = v^2/r$ where v is the velocity module and r is the local curvature radius. In our approach, it is convenient to express a_n by means of the expression

$$a_n = \boldsymbol{v} \cdot (\boldsymbol{v} \cdot \nabla)\,\boldsymbol{n}, \tag{7}$$

that is quadratic in the velocity components and where ∇ denotes the gradient operator. Taking advantage of Eq. (7), one can observe that in Eq. (6) the point acceleration $\boldsymbol{a}$ is expressed in terms of the driving gravity acceleration and of a_n, that depends on the local velocity. This property makes this

formalization suitable to solve the problem through a Runge–Kutta (RK) explicit method.

Since the point is supposedly constrained to move on a surface, the problem can be reduced to a two-degree-of-freedom formulation. Taking into account that from $z = f(x, y)$ it follows that the vertical velocity component v_z is given by

$$\dot{z} = v_z = f_x v_x + f_y v_y$$

and that the vertical acceleration component a_z has the form

$$\dot{v}_z = f_x \dot{v}_x + f_y \dot{v}_y + f_{xx} v_x^2 + 2 f_{xy} v_x v_y + f_{yy} v_y^2.$$

Equation (6) can be solved only for the horizontal components of the point acceleration a_x and a_y. Note that in the above expression the second-order derivatives of the function f have been denoted by f_{xx}, f_{xy}, and f_{yy}. After some manipulations, the governing set of equations becomes

$$\dot{v}_x = \psi(x,y)\left[\varphi(x,y) f_x + \mu\chi(x,y)\, v_x\right], \tag{8a}$$

$$\dot{v}_y = \psi(x,y)\left[\varphi(x,y) f_y + \mu\chi(x,y)\, v_y\right], \tag{8b}$$

where

$$\psi(x,y) = -\varphi(x,y)\left[g + \vartheta(x,y)\right], \tag{8c}$$

$$\varphi(x,y) = \left(1 + f_x^2 + f_y^2\right)^{-\frac{1}{2}}, \tag{8d}$$

$$\chi(x,y) = \left[v_x^2 + v_y^2 + (f_x v_x + f_y v_y)^2\right]^{-\frac{1}{2}}, \tag{8e}$$

$$\vartheta(x,y) = f_{xx} v_x^2 + 2 f_{xy} v_x v_y + f_{yy} v_y^2. \tag{8f}$$

2.2 Runge–Kutta method

To solve the above problem, we use an explicit RK4 numerical method. As is known, RK methods were conceived to solve first-order ODE of the type

$$\dot{\boldsymbol{w}} = \boldsymbol{F}(\boldsymbol{w}, t),$$

where t is the independent variable, and $\boldsymbol{w}$ and $\boldsymbol{F}$ may be N component vectors to represent a set of N differential equations. It is easy to see that the second-order ODE problem described by the set of Eq. (8) can be transformed into a first-order ODE, suitable for an RK application, if one poses

$$\boldsymbol{w} = (x, y, v_x, v_y)$$

and correspondingly poses

$$\boldsymbol{F} = \left[v_x, v_y, \psi(\varphi f_x + \mu\chi v_x), \psi(\varphi f_y + \mu\chi v_y)\right].$$

RK methods build the solution at the time t_{n+1} by means of an expression of the type

$$\boldsymbol{w}^{n+1} = \boldsymbol{w}^n + k\left(\beta_1 \tilde{\boldsymbol{F}}^{n+c_1} + \beta_2 \tilde{\boldsymbol{F}}^{n+c_2} + \ldots + \beta_s \tilde{\boldsymbol{F}}^{n+c_s}\right), \tag{9}$$

where $\boldsymbol{w}^n$ is the solution computed at the time t_n, k is the time step, β_s and c_s are suitable coefficients and $\tilde{\boldsymbol{F}}^{n+c_i} = \dot{\boldsymbol{w}}(t_{n+c_i})$. The coefficients c_i are such that all times t_{n+ci} lie in the interval between t_n and t_{n+1}. To compute the intermediate slopes $\tilde{\boldsymbol{F}}^{n+c_i}$ appearing in Eq. (9), intermediate values of $\tilde{\boldsymbol{w}}^{n+c_i}$ are needed. These are computed by adding increments to $\boldsymbol{w}^n$ that are linear combinations of the previously computed slopes $\tilde{\boldsymbol{F}}^{n+c_j}$ with $j < i$.

For the RK4 method adopted in this paper, $s = 4$ and the coefficients of Eq. (9) are

$$c_1 = 0,\ c_2 = 1/2,\ c_3 = 1/2,\ c_4 = 1,$$
$$\beta_1 = \frac{1}{6},\ \beta_2 = \frac{1}{3},\ \beta_3 = \frac{1}{3},\ \beta_4 = \frac{1}{6},$$

while the intermediate values $\tilde{\boldsymbol{w}}^{n+c_i}$ are computed as

$$\tilde{\boldsymbol{w}}^{n+c_i} = \boldsymbol{w}^n + k c_i \tilde{\boldsymbol{F}}^{n+c_{i-1}}.$$

2.3 Analytical solutions

The choice of the RK4 numerical method is based on a series of comparisons against analytical solutions obtained with RK schemes of different order. Basically, we obtained that RK4 is the lowest order RK method providing sufficiently accurate results. We give here only two examples, without and with friction. The solutions are computed through a MATLAB code.

2.3.1 Case 1

The first case we deal with as a test is a frictionless constant-velocity circular horizontal motion that takes place on the inner surface of a spherical cap, given by means of the equation

$$z = R - \sqrt{R^2 - x^2 - y^2}, \quad z < z_{max} \le R, \tag{10}$$

where R is the sphere radius. It is easy to show that a particle with initial position $P_0 = (0, y_0)$ and initial velocity $V_0 = (v_0, 0)$ describes a circular horizontal trajectory if

$$v_0^2 = g y_0^2 \left(R^2 - y_0^2\right)^{-\frac{1}{2}}. \tag{11}$$

One can obtain this condition by considering the point accelerations. If the plane tangent to the sphere at P_0 has slope ϑ_0, then the horizontal centripetal acceleration associated with the horizontal circular motion of the particle is given by

$$a_c = \frac{v_0^2}{R \sin\vartheta_0}.$$

On the other hand, the acceleration a_c results from the sum of the horizontal projections of the effective gravity acceleration $g \sin\vartheta_0 \cos\vartheta_0$ and of the centripetal acceleration pointing towards the center of the sphere $v_0^2 \sin\vartheta_0 / R$. Hence, one can write the equation

$$a_c = \frac{v_0^2}{R \sin\vartheta_0} = g \sin\vartheta_0 \cos\vartheta_0 + \frac{v_0^2}{R} \sin\vartheta_0$$

and deduce that

$$v_0^2 = gR \tan\vartheta_0 \sin\vartheta_0, \tag{12}$$

which is equivalent to Eq. (11).

The motion of the point-mass can be expressed in the form

$$x(t) = R\sin\vartheta_0\sin(\omega t), \quad y(t) = R\sin\vartheta_0\cos(\omega t),$$

where $\omega = v_0/(R\sin\vartheta_0)$ is the particle angular velocity.

We computed the solutions through three RK schemes, namely RK2, RK3, and RK4 for a given value of R = 20 m and $\vartheta_0 = 45°$. With this parameters choice the angular frequency results to be ω = 0.83 rad/s.

The difference between the values of the numerical radius $r(t) = \sqrt{x(t)^2 + y(t)^2}$ and the theoretical radius $R\sin\vartheta_0$ is shown in Fig. 1. The RK2 scheme provides the worst result showing a constant drift of the particle over the sphere cap. The RK3 solution shows a similar behavior, but with a smaller drift, whereas RK4 provides the best result with a normalized difference in the order of 10^{-6}.

The difference between the numerical and the exact values of the phase ωt is shown in Fig. 2. We estimate the phase discrepancy δ between the analytical ($\boldsymbol{r}_{an}$) and numerical ($\boldsymbol{r}_{num}$) horizontal-position unit vectors by using the cross product formula

$$\boldsymbol{r}_{an} \times \boldsymbol{r}_{num} = \sin\delta.$$

Hence, we can write

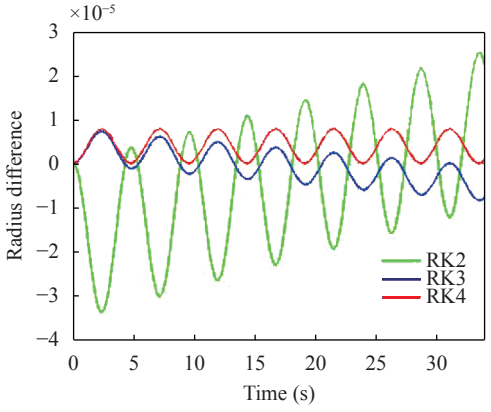

Fig. 1. Differences, normalized to $R\sin\theta_0$, between the analytical and numerical radius values for three RK schemes (Case 1).

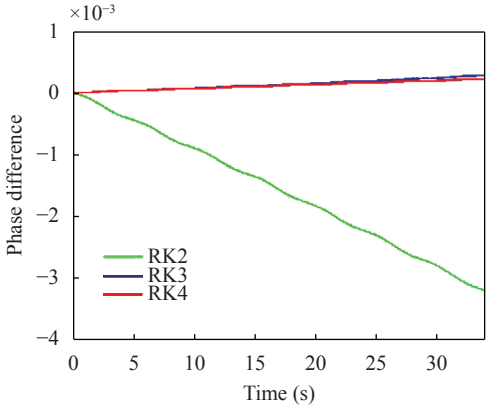

Fig. 2. Shift between the analytical and numerical phases for three RK schemes (Case 1).

$$\delta = \sin^{-1}\left(\frac{x_{an}y_{num} - y_{an}x_{num}}{R\sin\vartheta_0\sqrt{x_{num}^2 + y_{num}^2}}\right).$$

The best result is provided by the RK4 method. We observe that the RK2 solution is less accurate with maximum negative differences of 3.0×10^{-3}. The negative values indicate a delay in the particle motion with respect to the exact solution. The other two schemes perform similarly, with positive differences in the order of 10^{-4}.

For the sake of completeness, we also show the graph of the total energy in Fig. 3, which is constant and is given by

$$E_0 = gR(1 - \cos\vartheta_0) + \frac{1}{2}v_0^2$$

for a unit-mass particle. The relative error $e_r = \Delta E/E_0$, is defined as the ratio of the absolute value of the energy change ΔE to the initial energy E_0. By inspection, it is clear that the RK2 method gives the highest error values, in the order of 10^{-5}, while RK4 provides the best results, with relative errors in the range of 10^{-9}.

2.3.2 Case 2

The second test case is a one-dimensional (1D) motion over an inclined plane, under the effect of friction and gravity forces. The equation of the plane is $z = -x\tan\vartheta$, where the slope ϑ is a positive constant. If we impose that the motion occurs merely in the x-direction, the exact 1D solution for the particle horizontal displacement can be written in the form

$$x = x_0 + v_{0x}t + \frac{1}{2}g(\sin\vartheta \pm \mu\cos\vartheta)\cos(\vartheta t^2),$$

where x_0 is the initial position, v_{0x} is the initial horizontal velocity, μ is the friction coefficient, ϑ is the plane slope, and the sign of the friction term is negative when the motion is downslope and positive when it is upslope.

The grid used to represent the surface is built in the domain $x = [0:10] \times 10^3$ m and $y = [-2:+2] \times 10^3$ m. The initial positions and velocities are $P_0 = (5 \times 10^3, 0)$ m and $\boldsymbol{v}_0 = (-20, 0)$ m/s. The angle of the incline is $\vartheta = 5.7°$. We compute the numerical and analytical solutions until t = 300 s, with a time step dt = 0.05 s.

The normalized absolute difference between the values of $x(t)$ computed numerically and analytically is shown in Fig. 4.

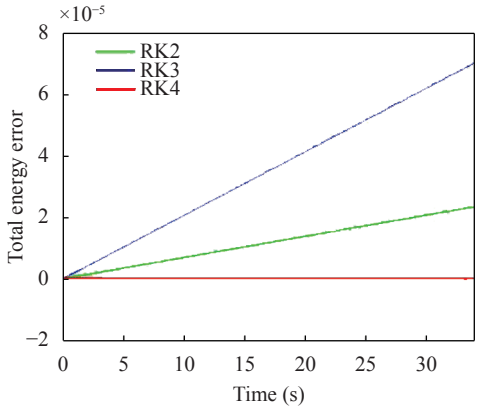

Fig. 3. Total energy errors for the used RK methods (Case 1).

The normalization factor is $\Delta x_{an} = \left|x_{fin}^{an} - x_{in}^{an}\right|$, where x_{fin}^{an} and x_{in}^{an} are the final and initial horizontal positions computed analytically. Given the selected parameters, the particle moves backward (and upslope) up to the turning time t = 19.6 s and then it moves forward (and downward) going beyond the initial position. RK2 provides the worst result with discrepancies up to 8×10^{-5}, while RK3 and RK4 produce results similar to each other, with differences more than 4 times smaller.

During its motion, the particle loses energy due to bottom friction. The absolute difference between the instantaneous analytical and numerical energies normalized to the analytical energy $E_{tot}^{an}(t)$ is shown in Fig. 5. RK2 shows differences in the order of 10^{-6}, while RK3 and RK4 in the order of 10^{-7}. Also in this latter case the results provided by RK3 and RK4 are essentially the same.

To sum up, all the RK methods provide acceptable solutions, but the RK4 scheme results to be the most accurate numerical method in terms of trajectory computations and system energy estimation and is, therefore, the one we have adopted for the rest of the paper.

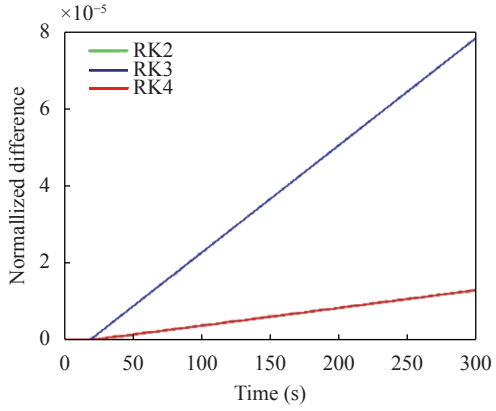

Fig. 4. Absolute differences between analytical and numerical positions, normalized to the total horizontal distance covered by the particle, for RK2, RK3, and RK4. Notice the increasing discrepancy after the turning time due to the inaccurate identification of the time instant where the velocity vanishes (Case 2).

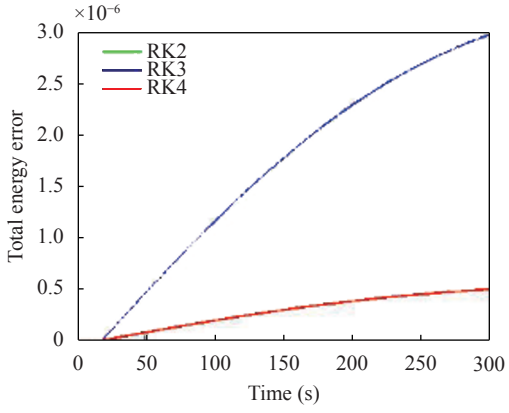

Fig. 5. Absolute differences, normalized to E_{tot}^{an}, between the total particle energies, computed analytically and numerically. Notice the increased discrepancies after the turning time (Case 2).

2.4 Examples

In addition to the test cases given in the previous section, we show simulations for which no analytical solutions are available. The space scale is in the order of kilometers, which is typical of geophysical landslide problems.

2.4.1 Example 1

The first bottom surface we take into account is described by the equation

$$z = ax^2 + by + c, \tag{13}$$

where the values of the coefficients are $a = 10^{-5}$ m^{-1}, $b = -5\times10^{-5}$ m^{-1}, and c = 10 m. Due to the surface shape, we will refer to it as a valley, that has a parabolic cross-section and a constant longitudinal mild slope (controlled by the coefficient b). The RK4 solution is computed until $t = 10^3$ s with a time step dt = 0.1 s. The starting position is (x_0 = –1600 m, y_0 = 0) m and the assumed initial velocity is (v_{x0} = 0, v_{y0} = 10) m/s. In the frictionless case we expect that the total system energy is constant. In Fig. 6 we show the particle trajectory (black thick line) on a contour map. The red point represents the starting position, while the range of the particle height is shown on the color bar on the right. As one can see, the mass is pushed downslope in the y-direction since v_{y0} is positive. For this surface, there is no analytical solution, but the expected motion is periodic along the x-direction (valley cross-section) and with uniform acceleration in the y-direction.

In Fig. 7, the relative error of the total system energy is shown. We calculate the error as $e_r = \Delta E/E_0$, where ΔE is the absolute difference of the instant energy $E(t)$ and the initial energy E_0. The error is very small, of the order of 10^{-15}, which confirms the good accuracy of the adopted RK4 method.

2.4.2 Example 2

The previous case is also treated under the assumption that there exists a friction force (with friction coefficient μ = 0.002). Figures 8 and 9 show the 2D trajectory and the energy decrease vs. time.

Friction has the effect of damping the oscillations in the x-direction. With the assumed parameters, the particle is expected to come eventually to a stop, but this occurs after we ended the simulation (that is after t = 1000 s).

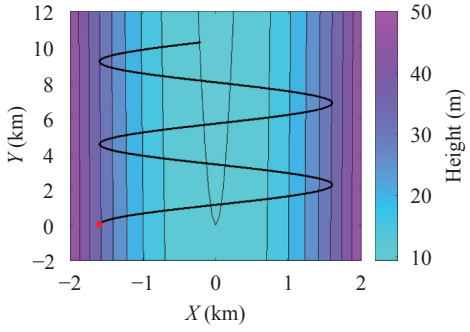

Fig. 6. Particle trajectory (thick black line) and initial position (red solid circle) in the case of a parabolic valley. The color bar on the right shows the vertical surface height z (Example 1).

3 Coupled masses

3.1 Formulation of the problem

In this section, we consider the motion of two coupled particles sliding on a 2D surface. We suppose that the two particles are connected to each other through a peculiar kind of interaction force, that keeps constant the geometrical distance between them.

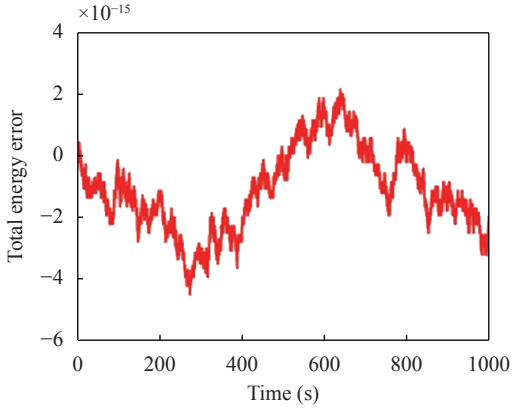

Fig. 7. Total-energy relative error (Example 1).

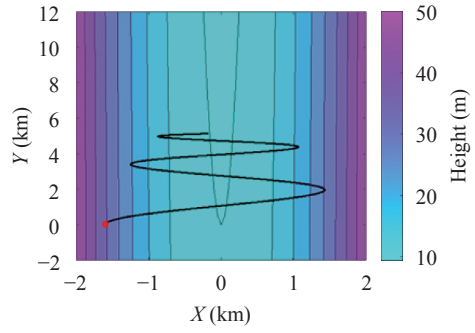

Fig. 8. Particle trajectory (thick black line) and initial position (red circle) in the bottom-friction case. The color bar on the right shows the vertical surface height z (Example 2).

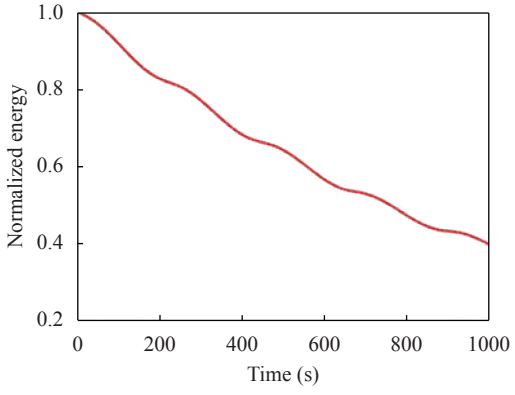

Fig. 9. Total energy normalized to the initial energy E_0 vs. time (Example 2).

The masses have the coordinates $\boldsymbol{r}_1$ and $\boldsymbol{r}_2$ in the space, and $\boldsymbol{x}_1$ and $\boldsymbol{x}_2$ in the horizontal Cartesian plane. Hence, their positions are $P_1 = (\boldsymbol{x}_1, f(\boldsymbol{x}_1))$ and $P_2 = (\boldsymbol{x}_2, f(\boldsymbol{x}_2))$.

We can write the constraint on their mutual distance through the dot product as

$$d_{12}^2 = (\boldsymbol{r}_1 - \boldsymbol{r}_2) \cdot (\boldsymbol{r}_1 - \boldsymbol{r}_2) = \text{Const}. \tag{15}$$

The equations of motion are

$$m_1 \ddot{\boldsymbol{r}}_1 = \boldsymbol{F}_1 + \boldsymbol{h}_{12} - (\boldsymbol{h}_{12} \cdot \boldsymbol{n}_1)\, \boldsymbol{n}_1, \tag{16a}$$

$$m_2 \ddot{\boldsymbol{r}}_2 = \boldsymbol{F}_2 - \boldsymbol{h}_{12} + (\boldsymbol{h}_{12} \cdot \boldsymbol{n}_2)\, \boldsymbol{n}_2, \tag{16b}$$

where m_1 and m_2 are the particle masses, and $\boldsymbol{F}_1$ and $\boldsymbol{F}_2$ are the external forces acting on the particles, namely gravity pointing downward, the reaction force due to the surface, pointing normal to the surface, and friction, pointing in the direction opposite to the motion. Further, $\boldsymbol{h}_{12}$ denotes the force exerted on the first particle by the second, and $\boldsymbol{h}_{21} = -\boldsymbol{h}_{12}$ is the one acting on the second particle by the first one. The last terms in Eq. (16) represent the surface reaction to the interaction force. In this paper we give a solution under the assumptions that they are negligible. This happens when the dot product between the interaction force and the local normals $\boldsymbol{n}_1$ and $\boldsymbol{n}_2$ is close to zero, i.e. when $\boldsymbol{h}_{12}$ forms a small angle with the plane that is tangent to the surface in the particle positions. Therefore, the equations of motions are approximated as follows

$$m_1 \ddot{\boldsymbol{r}}_1 = \boldsymbol{F}_1 + \boldsymbol{h}_{12}, \tag{17a}$$

$$m_2 \ddot{\boldsymbol{r}}_2 = \boldsymbol{F}_2 - \boldsymbol{h}_{12}. \tag{17b}$$

The complete theory of interacting particles moving on a surface is the subject of the companion paper [16].

The forces $\boldsymbol{F}_1$ and $\boldsymbol{F}_2$ depend on the position and velocity of the two particles. More precisely, the gravity force depends only on their position, while the reaction force and the friction force depend also on their velocity, as was shown in Sect. 2 where the equations governing the motion of a single particle have been derived. The interaction force $\boldsymbol{h}_{12}$ has a complicated expression. If we suppose that it is directed along the line joining the two particles, it can be given the following form

$$\boldsymbol{h}_{12} = h_{12} \frac{(\boldsymbol{r}_1 - \boldsymbol{r}_2)}{[(\boldsymbol{r}_1 - \boldsymbol{r}_2) \cdot (\boldsymbol{r}_1 - \boldsymbol{r}_2)]^{\frac{1}{2}}}\,.$$

After some algebraic manipulations that are fully given in the Appendix, it can be shown that $\boldsymbol{h}_{12}$ can be written as the sum of two parts, one depending on positions and velocities of the particles, and another depending also on their horizontal accelerations. More specifically, the general form of the interaction force can be written as

$$\boldsymbol{h}_{12} = (\boldsymbol{r}_1 - \boldsymbol{r}_2)\left[\Gamma_{12} - \Delta_{12}\left(f_{1x}\ddot{x}_1 + f_{1y}\ddot{y}_1 - f_{2x}\ddot{x}_2 - f_{2y}\ddot{y}_2\right)\right], \tag{18}$$

where Γ_{12} and Δ_{12} have expressions given in the Appendix. Here, it suffices to point out that, since Γ_{12} and Δ_{12} depend only on the mass positions and velocities, it follows that $\boldsymbol{h}_{12}$ is a linear function of the horizontal components of the accelerations.

After moving the linear terms containing the accelerations from the second to the first member of the system Eq. (17), we obtain a system of second-order differential equations. If we introduce the four-component vectors

$$\boldsymbol{q}^{\mathrm{T}} = [x_1, y_1, x_2, y_2],$$

$$\boldsymbol{b}^{\mathrm{T}} = [F_{1x} + (x_1 - x_2)\,\Gamma_{12}, F_{1y} + (y_1 - y_2)\,\Gamma_{12}, F_{2x} - (x_1 - x_2)\,\Gamma_{12}, F_{2y} - (y_1 - y_2)\,\Gamma_{12}].$$

Equation (17) can be given the compact form

$$\boldsymbol{A}\ddot{\boldsymbol{q}} = \boldsymbol{b},$$

where $\boldsymbol{A}$ is a 4 × 4 functions mass matrix (see Appendix) that depends on the positions and horizontal velocities of the masses, like the vector $\boldsymbol{b}$.

The system can be transformed into a first-order differential ODE by introducing the auxiliary variable $\boldsymbol{p}$, that is

$$\begin{aligned} \dot{\boldsymbol{q}} &= \boldsymbol{p}, \\ \dot{\boldsymbol{p}} &= \boldsymbol{A}^{-1}\boldsymbol{b}. \end{aligned} \tag{19}$$

Notice that the vector $\boldsymbol{q}$ can be interpreted as a generalized position vector of the two-particles system, since it identifies uniquely the system configuration. Likewise, $\boldsymbol{p}$ is the corresponding velocity vector. Equation (19) of the problem is suitable for RK method solution and we will solve it through an RK4 scheme that in Sect. 2 was shown to be adequate for the single particle dynamics. The general scheme for the discretization process is given by Eq. (9). The difference between the single particle case is that the unknowns are 8 instead of 4.

3.2 Analytical case

The above theory and numerical method can be tested against analytical solutions, that indeed exist only in very special cases. One of these is illustrated here.

3.2.1 Case 3

If we let two equal masses slide down on the constant-slope frictionless incline $z = -x\tan\vartheta$ under the effect of gravity and with equal and opposite initial velocities, we expect they spin around the center of mass of the system (CoM), that moves according to a parabolic law

$$x_c(t) = x_{c0} + \frac{1}{2} g \sin\vartheta \cos\left(\vartheta t^2\right),$$

$$y_c(t) = y_{c0},$$

$$z_c(t) = -x_c(t)\tan\vartheta,$$

where (x_{c0}, y_{c0}) is the initial position of the CoM on the horizontal plane. Let's take two equal particles with mass m placed at a distance d and symmetrically on the y-axis, i.e. $x_1(0) = x_2(0) = 0$, $y_1(0) = -y_2(0) = -d/2$, so that $x_{c0} = 0$ and $y_{c0} = 0$. Let's further assume that their initial velocities be equal, opposite and normal to the joining line, i.e. $v_{1x}(0) = -v_{2x}(0) = v$ and $v_{1y}(0) = v_{2y}(0) = 0$. It follows that the particles rotate with uniform speed $v/\cos\vartheta$ on the inclined plane around their CoM, and that their motion is described by the equations

$$\begin{aligned} x_1(t) &= x_c(t) + \frac{d}{2}\cos\vartheta \sin(\omega t), \\ y_1(t) &= -\frac{d}{2}\cos\vartheta\cos(\omega t), \\ z_1(t) &= -x_1(t)\tan\vartheta, \end{aligned}$$

$$\begin{aligned} x_2(t) &= x_c(t) - \frac{d}{2}\cos\vartheta \sin(\omega t), \\ y_2(t) &= \frac{d}{2}\cos\vartheta\cos(\omega t), \\ z_2(t) &= -x_2(t)\tan\vartheta. \end{aligned}$$

Here, $\omega = 2v/(d\cos\vartheta)$ is the angular velocity of the circular motion. Notice that at the same time the masses rotate around each other with the same frequency. In this case, however, the rotation radius and speed are d and $2v/\cos\vartheta$ respectively. The interaction force is exactly the force responsible for this rotation and can be proven to be equal to the centripetal force of a particle with mass $M_{12} = m/2$ (see definition in the Appendix), that is

$$h_{12} = -M_{12}\omega^2 d = 2mv^2/(d\cos^2 v). \tag{20}$$

In the numerical example, we set the slope angle ϑ to 0.6°. The initial positions are P_{01} = (0, –1000) m and P_{02} = (0, 1000) m. The two masses are equal ($m_1 = m_2$ = 10 kg). The initial velocities are $\boldsymbol{v}_{10}$ = (25, 0) m/s and $\boldsymbol{v}_{20}$ = (–25, 0) m/s.

The computed trajectories are displayed in Fig. 10. The accuracy of the solution is shown by plotting the normalized absolute difference between the analytical values of $x(t)$ and the values obtained through the RK4 method. The normalization factor is the radius of the circular motion $d/2$. Both particles show differences in the range of 10^{-11}, that is totally negligible.

Figure 12 displays the normalized difference between the numerical and the analytical distance that results to be in the order of 10^{-7}. The relative error in computing the interaction force h_{12} is plotted in Fig. 13 and happens to be remarkably small.

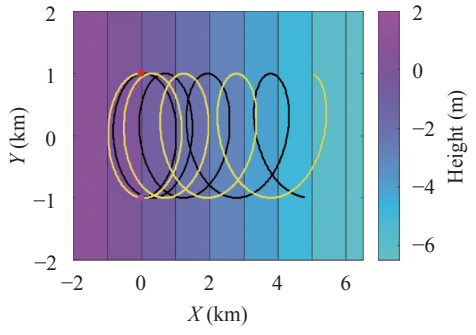

Fig. 10. Mass trajectories. Initial and final (t = 1000 s) positions are shown by circles and triangles. The black and yellow lines denote the first and second particles trajectories, respectively. Positions at the intermediate time t = 500 s are shown by diamonds (Case 3).

3.3 Examples

In this section, we treat two more cases of the coupled mass system that do not admit any analytical solutions and where the resulting trajectories are complex, even if the sliding surface is quite smooth.

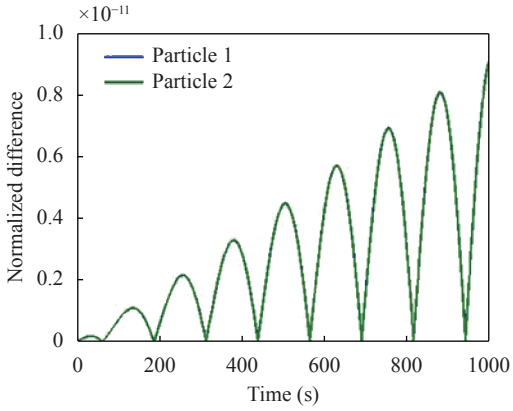

Fig. 11. Absolute differences between the x positions of the numerical (RK4) and of the analytical solutions, normalized to the radius of the circular motion around the system CoM (Case 3).

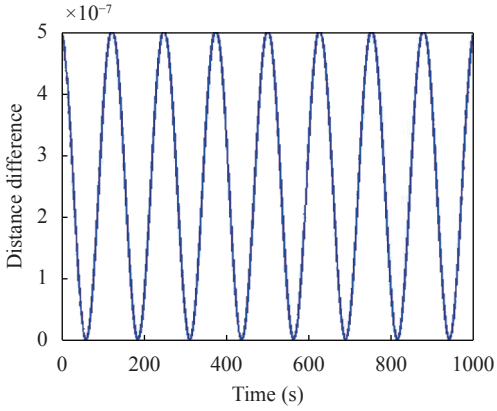

Fig. 12. Absolute difference between the analytical and the RK4-scheme inter-particle distance normalized to the analytical constant distance (Case 3).

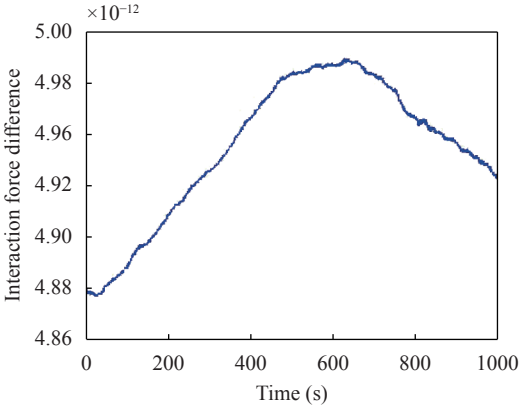

Fig. 13. Absolute difference between the analytical and the numerical interaction force, normalized to $|h_{12}|$ given by (Case 3).

3.3.1 Example 3

The selected bottom surface is described by the equation

$$z = ay^2 + bx + c,$$

where $a = 10^{-5}\,\mathrm{m}^{-1}$, $b = -5\times10^{-5}\,\mathrm{m}^{-1}$, $c = 10$ m, and can schematically represent a valley with a parabolic cross-section and a constant-slope axis. The bottom surface is supposedly frictionless.

The initial positions are in $P_{01} = (2000, -2000)$ m and $P_{02} = (2400, -1500)$ m. Initial velocities are all set to zero. Particles have masses: $m_1 = 100$ kg and $m_2 = 10$ kg. We will see that a considerable mass unbalance can lead to very irregular trajectories for the lighter mass, that is strongly influenced by the other as the effect of the interaction force.

The trajectories of the masses are plotted in Fig. 14. It can be noticed that the trajectory of the heavier particle shows a smoother path, while the trajectory of the other mass exhibits a series of highly complex transversal oscillations, with forward as well as backward motion, mainly due to the action of the interaction force.

There are invariants in the motion of the particles. The first is the distance between the particles, and the second is the total energy. Indeed, since the interaction force acts to keep the particle at a constant distance, it is responsible of the instant rotation of the masses around the CoM of the system and happens to be normal to their instant velocities. It follows that it does not perform any work on the system, and hence we expect that the total system energy, given by the sum of the total energies of the two masses, be conserved. As is evident in Fig. 15, the total system energy is constant with relative errors in the order of 10^{-6}. And Fig. 16 shows that the distance is conserved with a relative error in the order of 10^{-12}.

The interaction force changes with time. It is interesting to examine its behavior, that is displayed in Fig. 17, where it is normalized over the gravity force $m_1m_2g/(m_1+m_2)$. One can see that h_{12} completes more than 7 periods in about 1000 s. One could be tempted to relate the period of the interaction force to transversal oscillations of the masses, but the trajectory graph

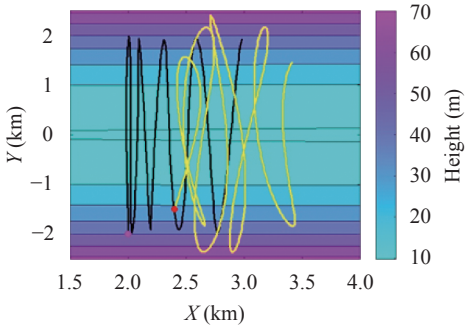

Fig. 14. Mass trajectories. Initial and final ($t = 2000$ s) positions are shown by circles and triangles. The black and yellow lines denote the first and second particles trajectories, respectively. Positions at the intermediate time $t = 1000$ s are shown by diamonds (Example 3).

(Fig. 14) shows that the motion along the flanks of the valley possesses a longer period and describes about 4.5 oscillations in the same 1000 s time interval. So what is remarkable is that in this example the particle motion is characterized by a double frequency: one due to the sliding down the cross-section and the other due to the interaction force. This changes from positive to negative regularly, which means that it passes from repulsive to attractive.

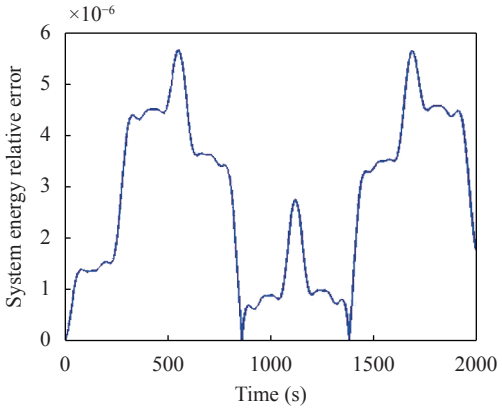

Fig. 15. Total system energy relative error in the absence of dissipative bottom friction (Example 3).

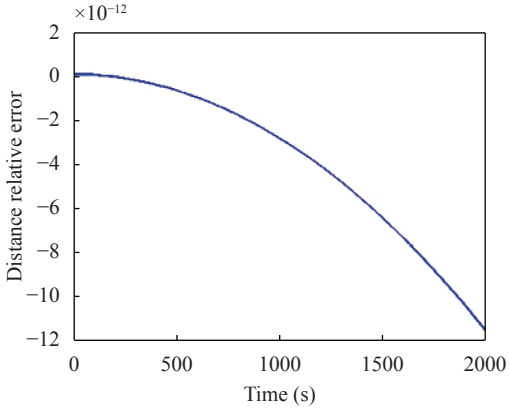

Fig. 16. Relative error of the inter-particle distance (Example 3).

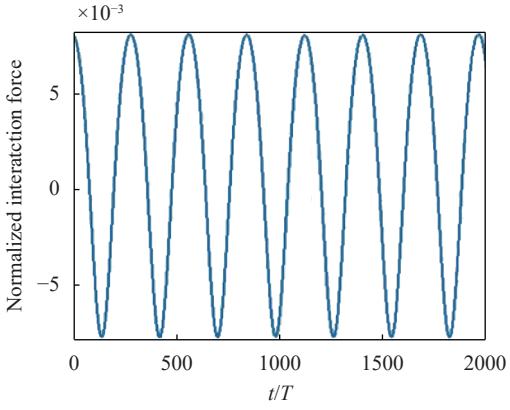

Fig. 17. Interaction force vs. time, normalized over $m_1 m_2 g/(m_1 + m_2)$ (Example 3).

3.3.2 Example 4

The case of Example 3 is also treated under the assumption that there exists a friction force ($\mu = 0.002$), all the rest remaining equal. Figure 18 portrays the trajectories for this case. Paths are similar to the ones of Example 3 (with no friction), but do not intersect and cover different regions. The lighter mass moves more irregularly, exhibiting also backward loops. There is an expected loss of energy due to the dissipation taking place at the surface, as is shown in Fig. 19, where the system total energy, normalized to the initial value E_0, is plotted. The RK4 solution keeps the inter-particle distance constant also in case of friction, with the relative error being in the order of 10^{-11}.

4 Conclusions

In this paper, we have treated the classical problem of a particle sliding on a surface, as well as the problem of a system of two particles coupled by means of an interaction force keeping constant their distance. In the former case the forces acting on the particle are gravity, the reaction force of the surface and the

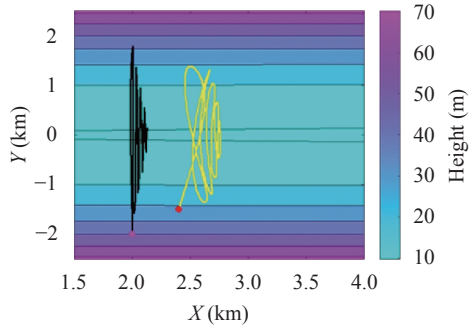

Fig. 18. Trajectory of two unequal coupled masses along a parabolic valley. Initial and final ($t = 2000$ s) positions are shown by circles and triangles. The black and yellow lines denote the first and second particles trajectories, respectively. Positions at the intermediate time $t = 1000$ s are shown by diamonds (Example 4).

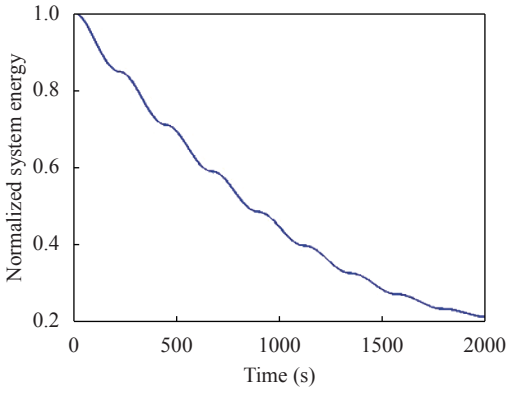

Fig. 19. Decay of the system total energy (normalised to the initial energy E_0) due to the bottom friction (Example 4).

surface friction. In the latter case, also the interaction force is active. The formulation of the first problem leads to a system of two second-order differential equations for the particle horizontal coordinates $x(t)$ and $y(t)$, that can be transformed into a four-equation RK scheme. The formulation of the second problem, which is original and fully given in the Appendix, leads to a system of four equations and to a corresponding eight-equation RK system.

In the paper, we have shown that the RK numerical method is adequate to solve the problem, but in order to obtain high-quality results at least a fourth-order scheme, that is an RK4, is required. This was proven by comparing numerical results obtained also with lower-order RK methods against analytical solutions with and without friction. Results for this comparison have been displayed in the paper only for the single particle cases, but tests have been run also for the coupled particles dynamics with identical conclusions.

The analytical cases we propose as comparison are simple, regarding constant slope planes or spherical cups, but some of them are not at all trivial, such as the cases of the mass travelling along a circular horizontal trajectory with constant speed (see Sect. 2.3) on the spherical cup, and the case of two particles sliding on a constant incline and rotating around each other (see Sect. 3.2). These analytical solutions can be seen as powerful benchmarks to measure the performance of any numerical method to solve particles sliding problems.

As regards the only analytical case for the two-particle system mentioned above, it is worth pointing out that it provides also the expression of the interaction force, which results to have a constant magnitude that is proportional to the mass M_{12}, to the square of the rotational velocity, and inversely proportional to the particles distance (see Eq. (20)). This expression is useful since it provides an order of magnitude for $|h_{12}|$ that is valid even for more complicated surfaces for which no analytical solutions exist, but that can be, even roughly, approximated by a constant incline.

The pure numerical examples given in the paper served the purpose to show that RK4 implemented code was accurate enough to conserve the constants of the motion (that is the energy, for frictionless motion, and the particle distance for coupled particles cases). We stress that the code can be used to treat any kind of initial conditions, and, moreover, in view of the very good results we obtained, it is expected to provide very accurate solutions even for complicated particles motions. Indeed, when the masses of the particles are very unbalanced, the lighter particle is expected to have a chaotic path around the more massive one along the slope, and a hint for this is the last case we treated in Sect. 3.3.

We have often used geological terms to describe surfaces, such as valley and depression. The reason for this is that this study is part of a research aiming at developing a new numerical code for landslides sliding down realistic mountain slopes, with the landslide represented as set of points (or blocks) interacting with each other. So, the final aim is to develop a theory and to implement a corresponding code handling N points with N being considerably larger than 2, with mutual links that might also be broken during the motion. This will allow us to simulate rockslides where blocks may fracture and break into fragment while sliding. If the focus is on geological slides, the role of friction and fragmentation is crucial and what matters most is the downslope fall phase, since no climbing of the landslide uphill does usually occur and no up-and-down oscillations across a valley are observed. We believe, however, that developing a complete code providing results even for frictionless constant-energy motion is a way to create a tool allowing for a better understanding of the basic physics and ultimately for more reliable simulations.

5 Acknowledgements

The research conducted in this paper was mostly financed by the FP7 Project ASTARTE “Assessment, Strategy and Risk Reduction for 740 Tsunamis in Europe” (FP7-ENV2013 6.4-3, Grant 603839) and by the Italian National Project RITMARE that, among others, treat landslide models with tsunamigenic potential.

References

[1] O. Hungr, A model for the runout analysis of rapid flow slides, debris flow, and avalanches, Can. Geotech. J. 32 (1995) 610–623.
[2] S. Tinti, C. Vannini, E. Bartolucci, A block-based theoretical model suited to gravitational sliding, Natural Hazards 16 (1997) 1–28.
[3] S.T. Grilli, P. Watts, Modelling of waves generated by moving submerged body. Applications to underwater landslide, Engineering Analysis with Boundary Elements 23 (1999) 645–656.
[4] P. Watts, Tsunami features of solid block underwater landslides, Journal of Waterways, Port, Coastal, and Ocean Engineering, 126, 144-152 126 (2000) 144–152.
[5] S. Tinti, G. Pagnoni, F. Zaniboni, The landslides and tsunamis of the 30th of December 2002 in Stromboli analysed through numerical simulations, Bull. Volcanol. 68 (2006) 462–479.
[6] A. Lucas, A. Mangeney, D. Mège, Influence of the scar geometry on landslide dynamics and deposits: Application to Martian landslides, Journal of Geophysical Research 116 (2011) E10001.
[7] G.E. Efremidis, M. Aulanitis, A. Konstantinidis, Realistic spring block model for earthquake induced landslide. in: 13th ISRM - International Society for Rock Mechanics, 2015.
[8] C.A. Stamatopoulos, B. Di, Analytical and approximate expressions predicting post-failure landslide displacement using the multi-block model and energy methods, Landslide 12 (2015) 1207–1213.
[9] C.A. Stamatopoulos, C. Mavromihalis, S. Sarma, Correction for geometry changes during motion of sliding-block seismic displacement., Journal of Geotechnical and Geoenvironmental Engineering 137 (2011) 926–938.
[10] V. Bandini, B. Biondi, E. Cascone, et al., GLE-based model for seismic displacement analysis of slopes including strength degradation and geometry rearrangement, Soil Dynamics and Earthquake Engineering 71 (2015) 128–142.
[11] E.T. Whittaker, A treatise on the analytical dynamics of particles and rigid bodies. Cambridge Unversity Press, 1988.
[12] J.B. Marion, Classical dynamics of particles and systems. Academic Press International Edition, 2013.
[13] J.C. Butcher, The numerical analyses of ordinary differential equations: Runge-Kutta and general linear methods. Wiley-Interscience, 1987.
[14] A. Wambecq, Rational Runge-Kutta methods for solving systems of ordinary differential equations, Computing 20 (1978)

333–342.
[15] E. Hairer, C. Lubich, M. Roche, The Numerical Solution of Differential-Algebraic Systems by Runge-Kutta Methods. Lecture Notes in Mathematics, 1989.
[16] S. Tinti, G. Gallotti, Numerical solutions for point masses sliding over analytical surfaces: Part 2, Theor. Appl. Mech. Lett., in press. DOI: 10.1016/j.taml.2019.02.005.

Appendix

Subtracting Eq. (17b) from Eq. (17a), we get

$$\ddot{\boldsymbol{r}}_1 - \ddot{\boldsymbol{r}}_2 = \frac{\boldsymbol{F}_1}{m_1} - \frac{\boldsymbol{F}_2}{m_2} + \frac{m_1+m_2}{m_1 m_2}\,\boldsymbol{h}_{12}.$$

After dot multiplying both members of Eq. (A.1) by $(\boldsymbol{x}_1 - \boldsymbol{x}_2)$, we obtain

$$\left(\ddot{\boldsymbol{x}}_1 - \ddot{\boldsymbol{x}}_2\right)\cdot(\boldsymbol{x}_1 - \boldsymbol{x}_2) = \left(\frac{\boldsymbol{F}_1}{m_1} - \frac{\boldsymbol{F}_2}{m_2}\right)\cdot(\boldsymbol{x}_1 - \boldsymbol{x}_2) + \frac{m_1+m_2}{m_1 m_2}\,\boldsymbol{h}_{12}\cdot(\boldsymbol{x}_1 - \boldsymbol{x}_2)\,. \tag{A.1}$$

On the other hand, if we derive Eq. (15) twice with respect to the time, we obtain

$$\left(\ddot{\boldsymbol{r}}_1 - \ddot{\boldsymbol{r}}_2\right)\cdot(\boldsymbol{r}_1 - \boldsymbol{r}_2) = -(\dot{\boldsymbol{x}}_1 - \dot{\boldsymbol{x}}_2)\cdot(\dot{\boldsymbol{x}}_1 - \dot{\boldsymbol{x}}_2) - (\dot{z}_1 - \dot{z}_2)^2\,,$$

which can be rewritten as

$$\left(\ddot{\boldsymbol{x}}_1 - \ddot{\boldsymbol{x}}_2\right)\cdot(\boldsymbol{x}_1 - \boldsymbol{x}_2) = -(\dot{\boldsymbol{x}}_1 - \dot{\boldsymbol{x}}_2)\cdot(\dot{\boldsymbol{x}}_1 - \dot{\boldsymbol{x}}_2) - (\dot{z}_1 - \dot{z}_2)^2 - (\ddot{z}_1 - \ddot{z}_2)\,(z_1 - z_2)\,. \tag{A.2}$$

After replacing Eq. (A.1) in Eq. (A.2), we can write

$$\frac{m_1+m_2}{m_1 m_2}\,\boldsymbol{h}_{12}\cdot(\boldsymbol{x}_1 - \boldsymbol{x}_2) = -\left(\frac{\boldsymbol{F}_1}{m_1} - \frac{\boldsymbol{F}_2}{m_2}\right)\cdot(\boldsymbol{x}_1 - \boldsymbol{x}_2) - (\dot{\boldsymbol{x}}_1 - \dot{\boldsymbol{x}}_2)\cdot(\dot{\boldsymbol{x}}_1 - \dot{\boldsymbol{x}}_2) - (\dot{z}_1 - \dot{z}_2)^2 - (\ddot{z}_1 - \ddot{z}_2)\,(z_1 - z_2)\,. \tag{A.3}$$

If we assume that the interaction force $\boldsymbol{h}_{12}$ lies on the direction joining the two particles, we can write the following expression

$$\boldsymbol{h}_{12} = h_{12}\,\frac{(\boldsymbol{r}_1 - \boldsymbol{r}_2)}{[(\boldsymbol{r}_1 - \boldsymbol{r}_2)\cdot(\boldsymbol{r}_1 - \boldsymbol{r}_2)]^{\frac{1}{2}}}\,. \tag{A.4}$$

Substituting Eq. (A.4) into Eq. (A.3), we obtain the scalar h_{12} that is positive when the force points towards the first particle, and negative if the force points towards the second particle

$$h_{12} = -\frac{m_1 m_2}{m_1+m_2}\,\frac{[(\boldsymbol{r}_1 - \boldsymbol{r}_2)\cdot(\boldsymbol{r}_1 - \boldsymbol{r}_2)]^{\frac{1}{2}}}{(\boldsymbol{x}_1 - \boldsymbol{x}_2)\cdot(\boldsymbol{x}_1 - \boldsymbol{x}_2)} \left[\left(\frac{\boldsymbol{F}_1}{m_1} - \frac{\boldsymbol{F}_2}{m_2}\right)\cdot(\boldsymbol{x}_1 - \boldsymbol{x}_2) + (\dot{\boldsymbol{x}}_1 - \dot{\boldsymbol{x}}_2)\cdot(\dot{\boldsymbol{x}}_1 - \dot{\boldsymbol{x}}_2) + (\dot{z}_1 - \dot{z}_2)^2 + (\ddot{z}_1 - \ddot{z}_2)\,(z_1 - z_2)\right]. \tag{A.5}$$

Considering that vertical velocities and accelerations can be expressed by means of their horizontal counterparts, i.e.

$$\dot{z} = v_z = f_x v_x + f_y v_y \dot{v}_z = f_x \dot{v}_x + f_y \dot{v}_y + f_{xx} v_x^2 + 2 f_{xy} v_x v_y + f_{yy} v_y^2$$

and making use of Eq. (A.4), the interaction force takes the form

$$\boldsymbol{h}_{12} = -\frac{m_1 m_2}{m_1+m_2}\,\frac{(\boldsymbol{r}_1 - \boldsymbol{r}_2)}{(\boldsymbol{x}_1 - \boldsymbol{x}_2)\cdot(\boldsymbol{x}_1 - \boldsymbol{x}_2)} \left[\gamma_{12} + (f_{1x}\ddot{x}_1 + f_{1y}\ddot{y}_1 - f_{2x}\ddot{x}_2 - f_{2y}\ddot{y}_2)\,(z_1 - z_2)\right], \tag{A.6}$$

where γ_{12} is a complicated expression depending only on the positions and horizontal velocities of the two particles, that is

$$\begin{aligned}\gamma_{12} = {} & \left(\frac{\boldsymbol{F}_1}{m_1} - \frac{\boldsymbol{F}_2}{m_2}\right)\cdot(\boldsymbol{x}_1 - \boldsymbol{x}_2) + (\dot{\boldsymbol{x}}_1 - \dot{\boldsymbol{x}}_2)\cdot(\dot{\boldsymbol{x}}_1 - \dot{\boldsymbol{x}}_2) \\ & + (f_{1x}\dot{x}_1 + f_{1y}\dot{y}_1 - f_{2x}\dot{x}_2 - f_{2y}\dot{y}_2)^2 \\ & + \left(f_{1xx}\dot{x}_1^2 + 2 f_{1x} f_{1y}\dot{x}_1\dot{y}_1 + f_{1yy}\dot{y}_1^2 - f_{2xx}\dot{x}_2^2\right. \\ & \left. - 2 f_{2x} f_{2y}\dot{x}_2\dot{y}_2 - f_{2yy}\dot{y}_2^2\right)(z_1 - z_2)\,.\end{aligned} \tag{A.7}$$

In Eq. (A.7) and hereafter, by f_{1x} and f_{1y} we denote the first derivative of the surface function f with respect to the space coordinates x and y, evaluated in the position of particle 1. Likewise, f_{2x} and f_{2y} are the derivatives taken in the position of the second particle. And similar notation is used for the second derivatives. It is worth observing that $\gamma_{12} = \gamma_{21}$, that is it does not change if one exchanges the position of the two particles. After introducing the following definitions

$$M_{12} = \frac{m_1 m_2}{m_1+m_2}\,, \tag{A.8}$$

$$\Gamma_{12} = -M_{12}\,\frac{\gamma_{12}}{(\boldsymbol{x}_1 - \boldsymbol{x}_2)\cdot(\boldsymbol{x}_1 - \boldsymbol{x}_2)}\,, \tag{A.9}$$

$$\Delta_{12} = M_{12}\,\frac{z_1 - z_2}{(\boldsymbol{x}_1 - \boldsymbol{x}_2)\cdot(\boldsymbol{x}_1 - \boldsymbol{x}_2)}\,. \tag{A.10}$$

Equation (A.4) can be given the compact form

$$\boldsymbol{h}_{12} = (\boldsymbol{r}_1 - \boldsymbol{r}_2)\left[\Gamma_{12} - \Delta_{12}\,(f_{1x}\ddot{x}_1 + f_{1y}\ddot{y}_1 - f_{2x}\ddot{x}_2 - f_{2y}\ddot{y}_2)\right]. \tag{A.11}$$

It is important to stress that, strictly speaking, due to the way it was derived, the expression (A.11) does not ensure that the particle distance is constant during the motion, but rather that its second derivative with respect to time is zero (see Eq. (A.2)). This means that it is allowed to change with a constant rate, and if the initial conditions are suitable, it remains constant (for instance, if the particles initial velocities are assumed to be zero). Observe further that from the above definitions (A.8)–(A.10), it follows that $M_{12} = M_{21}$, $\Gamma_{12} = \Gamma_{21}$, but $\Delta_{12} = -\Delta_{21}$. Using Eq. (A.11) for the interaction force, the equations of motion for the two particles along the horizontal axes x and y can be written as

$$\begin{aligned}&[m_1 + (x_1 - x_2)\,\Delta_{12} f_{1x}]\,\ddot{x}_1 + (x_1 - x_2)\,\Delta_{12} f_{1y}\ddot{y}_1 \\ &\quad - (x_1 - x_2)\,\Delta_{12} f_{2x}\ddot{x}_2 - (x_1 - x_2)\,\Delta_{12} f_{2y}\ddot{y}_2 = F_{1x} + (x_1 - x_2)\,\Gamma_{12},\end{aligned}$$

$$\begin{aligned}&(y_1 - y_2)\,\Delta_{12} f_{1x}\,\ddot{x}_1 + [m_1 + (y_1 - y_2)\,\Delta_{12} f_{1y}]\,\ddot{y}_1 \\ &\quad - (y_1 - y_2)\,\Delta_{12} f_{2x}\,\ddot{x}_2 - (y_1 - y_2)\,\Delta_{12} f_{2y}\ddot{y}_2 = F_{1y} + (y_1 - y_2)\,\Gamma_{12},\end{aligned}$$

$$
\begin{aligned}
&-(x_1-x_2)\,\Delta_{12}f_{1x}\,\ddot{x}_1-(x_1-x_2)\,\Delta_{12}f_{1y}\,\ddot{y}_1\\
&\quad+[m_2+(x_1-x_2)\,\Delta_{12}f_{2x}]\,\ddot{x}_2+(x_1-x_2)\,\Delta_{12}f_{2y}\,\ddot{y}_2\\
&\quad=F_{2x}-(x_1-x_2)\,\Gamma_{12},
\end{aligned}
$$

$$
\begin{aligned}
&-(y_1-y_2)\,\Delta_{12}f_{1x}\,\ddot{x}_1-(y_1-y_2)\,\Delta_{12}f_{1y}\,\ddot{y}_1+(y_1-y_2)\,\Delta_{12}f_{2x}\,\ddot{x}_2\\
&\quad+[m_2+(y_1-y_2)\,\Delta_{12}f_{2y}]\,\ddot{y}_2=F_{2y}-(y_1-y_2)\,\Gamma_{12}.
\end{aligned}
$$

This is a system of second-order differential equations in the four unknown functions x_1, y_1, x_2, and y_2 that can be formally written as

$$\boldsymbol{A}\,\ddot{\boldsymbol{q}}=\boldsymbol{b},$$

where

$$\boldsymbol{q}^{\mathrm{T}}=[x_1,\ y_1,\ x_2,\ y_2]\,,$$

$$
\begin{aligned}
\boldsymbol{b}^{\mathrm{T}}=[&F_{1x}+(x_1-x_2)\,\Gamma_{12},\ F_{1y}+(y_1-y_2)\,\Gamma_{12},\\
&F_{2x}-(x_1-x_2)\,\Gamma_{12},\ F_{2y}-(y_1-y_2)\,\Gamma_{12}]\,.
\end{aligned}
$$

Notice that the four-component vector $\boldsymbol{b}^{\mathrm{T}}$, which has the dimension of a force, contains only masses, positions and horizontal velocities of the particles, and accounts for the forces $\boldsymbol{F}_1$ and $\boldsymbol{F}_2$. The mass matrix $\boldsymbol{A}$ has the form

$$
\boldsymbol{A}=\begin{bmatrix}
m_1+(x_1-x_2)\,\Delta_{12}f_{1x} & (x_1-x_2)\,\Delta_{12}f_{1y} & -(x_1-x_2)\,\Delta_{12}f_{2x} & -(x_1-x_2)\,\Delta_{12}f_{2y}\\
(y_1-y_2)\,\Delta_{12}f_{1x} & m_1+(y_1-y_2)\,\Delta_{12}f_{1y} & -(y_1-y_2)\,\Delta_{12}f_{2x} & -(y_1-y_2)\,\Delta_{12}f_{2y}\\
-(y_1-y_2)\,\Delta_{12}f_{2y} & -(x_1-x_2)\,\Delta_{12}f_{1y} & m_2+(x_1-x_2)\,\Delta_{12}f_{2x} & (x_1-x_2)\,\Delta_{12}f_{2y}\\
-(y_1-y_2)\,\Delta_{12}f_{1x} & -(y_1-y_2)\,\Delta_{12}f_{1y} & (y_1-y_2)\,\Delta_{12}f_{2x} & m_2+(y_1-y_2)\,\Delta_{12}f_{2y}
\end{bmatrix}
$$

and depends on particles masses and positions.